SEMARAK ILMU PUBLISHING

CFD Letters

Journal homepage:
https://semarakilmu.com.my/journals/index.php/CFD_Letters/index
ISSN: 2180-1363

The Effect of Tortuosity on Wall Shear Stress of Porous Scaffold

Hasan Basri[1], Akbar Teguh Prakoso [1], Zainal Abidin[1], Ardiansyah Syahrom[2,3], Imam Akbar [4], Dendy Adanta[1,*]

[1] Department of Mechanical Engineering, Faculty of Engineering, Universitas Sriwijaya, Ogan Ilir-30662, South Sumatera, Indonesia
[2] Applied Mechanics and Design, School of Mechanical Engineering, Faculty of Engineering, Universiti Teknologi Malaysia, 81310 UTM Johor Bahru, Malaysia
[3] Medical Devices and Technology Centre (MEDiTEC) Institute of Human Centred and Engineering (iHumEn), Universiti Teknologi Malaysia, 81310 UTM Johor Bahru, Malaysia
[4] Department of Mechanical Engineering, Faculty of Engineering, Tridinanti University, Palembang 30129, South Sumatra, Indonesia

ARTICLE INFO

Article history:
Received 16 December 2022
Received in revised form 14 January 2023
Accepted 15 February 2023
Available online 1 July 2023

Keywords:
Scaffold; Negative Schwarz P; Permeability; Wall Shear Stress; Tortuosity.

ABSTRACT

This study aimed to investigate the effect of morphology on permeability and fluid wall shear stress of porous scaffold. Fluids passing through the scaffold were analyzed using the computational fluid dynamics (CFD) method, and tortuosity was analyzed using the finite-different analysis (FDA) method. Based on the results, the higher the porosity, the higher the permeability. In contrast, by increasing the tortuosity, the permeability decrease. Then, control curvature in the negative Schwarz p design has the potential to increase the permeability, consequently, decrease the specific surface area. Therefore, the design negative Schwarz p was proposed met the requirements for a good implant which the permeability value was in the range of trabecular bone.

1. Introduction

The phenomenon of mass transport in porous media has been studied comprehensively to understand the transport mechanisms and their impact on structural properties. The application of the theory of porous media to biological tissues has led to significant advances in analyzing the structural characteristics of biomaterials for the diffusion of nutrients [1–3]. The trabecular bone forms a network that is not a regular lattice in the form of straight lines like the skeleton. In contrast, nature chooses a tortuous structural design that presents bone tissue that is strongly connected to the aspects of the rods and plates. Consequently, a detailed understanding of the structure and properties of the complex porous system and its influence on the mechanism of mass transport can contribute to the development of scaffold biomaterials for tissue engineering. The contribution of scaffold biomaterials addresses crucial problems, including changes in bone tissue due to degenerative pathologies, such as osteoporosis and osteoarthritis [4-5].

Regarding trabecular bone tissue, this bone complexity has a fundamental function that contributes to the micro-regulation of blood circulation [6]. Hence, the porous media to describe this

* *Corresponding author.*
E-mail address: dendyadanta@ymail.com (Dendy Adanta)

https://doi.org/10.37934/cfdl.15.7.6173

complexity will be very relevant if it is referred to as tortuosity to be used as a parameter in developing scaffold biomaterials. Tortuosity is a pattern or structure that deviates from its square shape. Therefore, this study focuses on the tortuosity parameter to determine the effect on permeability. Based on a study by Bobbert *et al.*, [7], controlling tortuosity can modulate bone tissue formation significantly. Hence, the tortuosity parameter is important for investigating the wall's permeability and shear stress. The permeability has been shown to directly contribute to cell migration in the scaffold and vascularization [8]. In addition, fluid-induced wall shear stress (WSS) plays a significant role in the differentiation and proliferation of cells in perfusion bioreactors that include a relatively more dynamic cell culture system [9]. The contribution of WSS to the differentiation of pluripotent stem cells toward endothelial [10], cardiac [11], hematopoietic [12], and osteoblast phenotypes [13].

The previous study hypothesizes that tortuosity is correlated with specific surface area and WSS; the phenomenon of nutrient transport and the interaction between fluid and surface area will be much increased, and the consequence makes a slowdown in the velocity of the fluid through the scaffold. Consequently, increased fluid pressure on the scaffold decreases the permeability, and tortuosity decreases porosity increases. However, the porosity does not wholly affect the tortuosity; there is a condition where the tortuosity becomes an independent parameter. Therefore, it is necessary to study the tortuosity of nutrient transport comprehensively.

The design potential in the development of bone scaffolds with various variations of tortuosity-this topic does not yet have attention from the previous study that has developed a bone scaffold model that can control curvature; tortuosity without affecting porosity. Allegedly, the controllable curvature can make the same porosity, and the tortuosity value can differ. Thus, this study aims to investigate the effect of morphological porosity and tortuosity on permeability and WSS by utilizing computational simulations. As for the biomaterial scaffold that we used, we named it negative Schwarz primitive (NSP).

2. Material and Method

2.1 Parametric Design of Scaffold and Cancellous Bone Reconstruction

The scaffold model used in this study is open porous based on the tortuous pathway in a fluid channel designed by commercial CAD software. The tortuosity identically open-channel flows (twisted; having many turns). Therefore, this model to developed to understand the basic role of the tortuosity parameter on transfer phenomena properties, especially permeability in the porous scaffold. Figure 1 shows the schematic diagram scaffold build design. Based on Figure 1, the fluid geometry was generated using parametric study: For A-dimensional parametric study to generate unit cell various porosity (Table 1); For B-multiple meandering fluid channels interconnected geometry created. For C and D-the Boolean operations subtracting between the internal and the external contours gave the final 3D porous interconnected structure; For E-various unit cells with different porosity can be obtained by adjusting the fluid pore size (X value).

Each geometry was labelled after the structure, porosity, and curvature. For example, NSP25 refers to the Negative Schwarz Primitive curvature of 0.4 scaffolds with 25% porosity, NSP25Dr1 refers to the Negative Schwarz Primitive scaffold with a curvature of 0.45 and porosity of 25%, and NSP25Dr1 refers to the Negative Schwarz Primitive scaffold with curvature 0.49 and porosity 25%.

Table 1
Dimension parameter features of the Negative Schwarz P model CAD design

Dimensional parametric study	Value		
Model	NSP	NSPDr1	NSPDr2
r	0.4	0.45	0.49
constant, *c*		0.745	
y		2c-r	
z		c-(r/2)	
t		2.1	
x (Φ: 25%)	0.45	0.421	0.41
x (Φ: 35%)	0.54	0.515	0.51
x (Φ: 45%)	0.62	0.603	0.6
x (Φ: 50%)	0.66	0.646	0.645
x (Φ: 60%)	0.74	0.731	0.735
x (Φ: 65%)	0.78	0.775	0.778

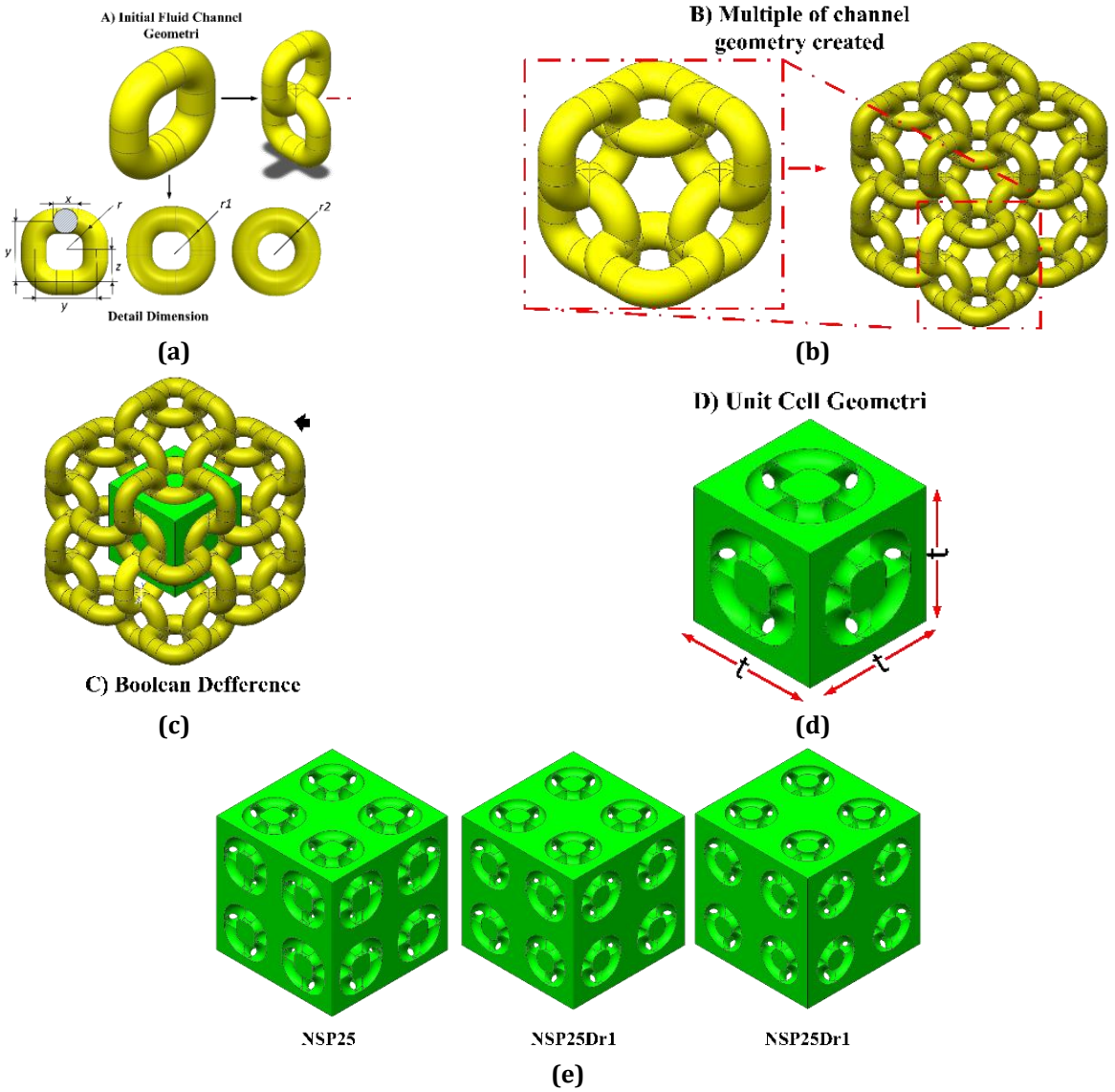

Fig. 1. Schematic diagram process showing the scaffold design principle based on the meandering pore method: (a) Fluid channel geometry; (b) Then after, the geometry duplicates interconnected; (c) Assembly of the fluid geometry and a cubic by Boolean operation; (d) Final unit cell; and (e) Final scaffold

2.2 Computational Fluid Dynamics (CFD) Method

The CFD analysis using COMSOL Multiphysics ® Software Burlington, USA [14]. The model scaffold size of 4.2×4.2×4.2 mm with a fluid domain size of 6.2×4.2×4.2 mm. Then, the fluid model is simulated body fluid (SBF) where the dynamic viscosity (μ) value is 0.001 Pa·s and the density of 1 g/cm^3 [15]. The fluid flow is assumed as incompressible flow (Eq. (1)) with the inlet of 6.67 ml/min with the boundary between the fluid and solid-defined no-slip conditions. The Navier-stokes relation for fully developed flow on incompressible fluid dynamics with constant density and viscosity was used in CFD analysis [16], as follows:

$$\rho\frac{\partial u}{\partial t}-\mu\nabla^2 u+\rho(u\cdot\nabla)u+\nabla p=F \tag{1}$$

where ρ is the fluid density (kg/m^3), u is the velocity of the fluid (m/s), ∇ is a del operator (∇·u=0), p is the pressure (Pa), and F denotes other forces (gravity or centrifugal force) (in case of F = 0).

Then, the pressure on the outlet is set to 0 Pa, and the average pressure in the inlet represents a pressure drop (Δp). After Δp is obtained, each porous scaffold permeability and wall shear stress are evaluated using (Eq. (2) and (3)). The permeability of the different scaffolds was calculated based on the pressure drop across the structure using Darcy's Law [17], which can be expressed as follows:

$$\mathrm{K}=\frac{\mathrm{Q}\cdot\mu\cdot L}{A\cdot\Delta p} \tag{2}$$

where K is the permeability (m^2), Δp is the pressure drops across the structure (Pa), L is the length of the section (mm), A is the cross-sectional area of the flow (m^2), and Q is the flow rate or discharge (m^3/s).

For laminar flow, the wall shear stress (τ_w) represents the tangential drag force exerted by the fluid flowing across the surface of the scaffold and is given by:

$$\tau_w=\mu\frac{\partial u}{\partial n} \tag{3}$$

Where μ is the dynamic viscosity of the fluid (Pa·s), and n is the x-,y- and z-direction (m). Figure 2 shows the boundary conditions set in the model.

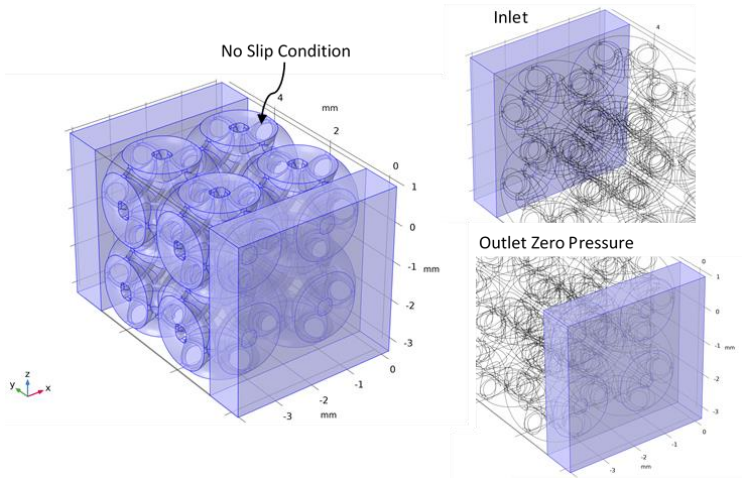

Fig. 2. Finite element boundary condition

2.3 Convergence Mesh Method

The u is the parameter for the mesh sensitivity test using the grid convergency index (GCI) analysis [18]. An example of GCI calculation is:

$$\mathrm{GCI} = \mathrm{F_s}\left|\frac{1}{u_{\mathrm{finer}}}\frac{u_{\mathrm{finest}}-u_{\mathrm{finer}}}{r_{\mathrm{ff}}^{\,\mathrm{q_n}}-1}\right|\cdot 100\% \tag{4}$$

F_s is the safety factor of 1.25, r is the grid refinement ratio, and q is the convergency observed order. The numerical calculation of q is:

$$\mathrm{q_{n+1}} = \ln\left|\left(\frac{u_{\mathrm{fine}}-u_{\mathrm{finer}}}{u_{\mathrm{finer}}-u_{\mathrm{finest}}}\left(r_{\mathrm{fsfr}}^{\,\mathrm{q_n}-1}\right)\right)+r_{\mathrm{fsfr}}^{\,\mathrm{q_n}}\right| / \ln\left(r_{\mathrm{fsfr}}\cdot r_{\mathrm{frf}}\right) \tag{5}$$

And for the r calculation is:

$$r_{\mathrm{ff}} = \left(\frac{\mathrm{M}_{finer}}{\mathrm{M}_{finest}}\right)^{0.5} \tag{6}$$

M is the mesh number. Then, the mesh number is normalized by inverse comparison. The example of normalized mesh number (h) is:

$$\mathrm{h_{finest}} = \mathrm{h}_{finer}\cdot r_{ff} \tag{7}$$

Where h_{finer} of 1. The u_{exact} or $u_{\Delta x\to\sim}$ or is predicted using the extrapolation approach. The formulation for extrapolation is:

$$u_{\Delta x\to 0} = u_{\mathrm{finer}} - \left(\frac{u_{\mathrm{finest}}-u_{\mathrm{finer}}}{r_{\mathrm{ff}}^{\,\mathrm{q_n}+1}-1}\right) \tag{8}$$

2.4 Morphology Calculation Method

The porous scaffold morphological measurements using image analysis (FIJI image j) application Bone j and MATLAB (Mathworks Inc) application Taufactor. The calculation is based on the finite difference method (FDM), as the director uses image voxels as the discretization mesh for simulation. The STL porous scaffold was imported to a slicer software program (ChiTuBox, CBD-Tech) then 3D images were made into 420 slices. Then, the images are analyzed using Fiji image j and Taufactor with stages (i) adjusting brightness, (ii) applying a threshold, and (iii) removing noise using the "remove outliers" function. And for accurate calculation is done by entering the appropriate voxel size so that the length, width, and height are the same as the actual size.

3. Results and Discussion

3.1 GCI Calculation Result

Five mesh numbers are compared to find out the optimum mesh number: 56.8k (coarse), 118.6k (medium), 2,254k (fine), 3,690k (finer), and 4,770k (finest). Based on the calculation using Eq. (6), the

r_{fsfr} is 1.14, r_{frf} is 1.28, r_{fm} is 1.38, and r_{mc} is 1.44. Then, convert r to h, for: h_{fs} of 1, h_{fr} of 1.14, h_f of 1.45, h_m of 2.01, and h_c of 2.9. Based on CFD results, the u of each mesh is 5.148×10^{-2} m/s (coarse), 5.077×10^{-2} m/s (medium), 5.004×10^{-2} m/s (fine), 4.966×10^{-2} m/s (finer), and 4.963×10^{-2} m/s (finest).

Further, based on using Eq. (5), the q_n of 8.018. Then, using Eq. (8), the exact value ($u_{\Delta x\to\sim}$) from the extrapolation approach of 4.96×10^{-2} m/s. Finally, using Eq. (4), the GCI_{fsfr} of 0.05%, the GCI_{frf} of 0.15%, the GCI_{fm} 2.38%, and the GCI_{mc} of 3.78%. Therefore, the mesh number of 3,690k was chosen since, based on GCI results has an error below 1%. A summary of the GCI calculation results can be seen in Figure 3.

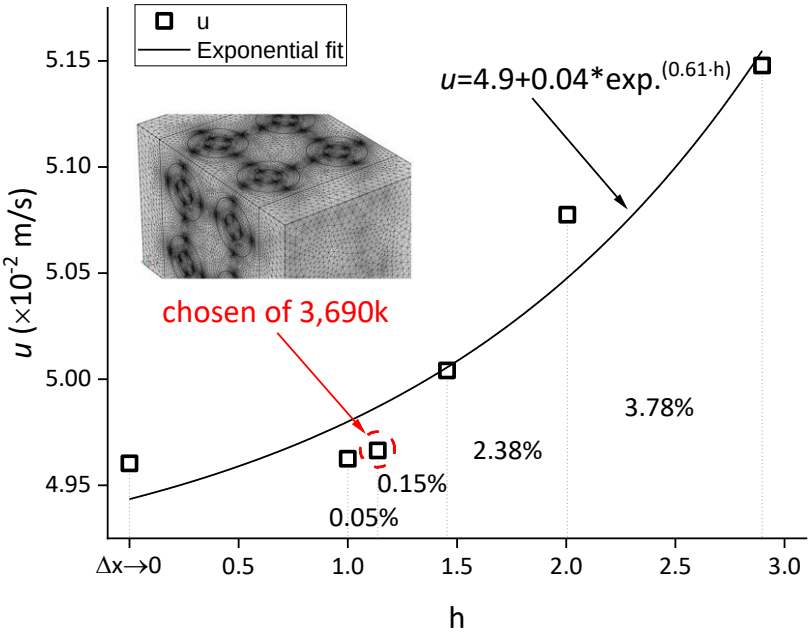

Fig. 3. Mesh sensitivity study on NSP scaffold

3.2 Morphology Analysis Results

Figure 4 shows the relation of the porosity to the tortuosity of a porous scaffold. Based on Figure 4, the relation of each model is linear, where the tortuosity increases and the porosity percentage decrease. From Figure 4, the NSP model has a higher tortuosity than the NSPDr1 and NSPDr2 models. Figure 4 means that the pores' size increased, the radius of curvature of the scaffold decreased, and the tortuosity increased. The porosity percentage for the cubic structure does not affect tortuosity (no change).

Figure 5(a) shows the relationship between the average trabecular thickness (Tb.Th) and separation (Tb.Sp) and porosity for the NSP scaffold model. Figure 5(a) shows increasing porosity, Tb.Sp increase and Tb.Th would decrease. For the same porosity, by increasing the pore size and reducing the radius of curvature, the Tb.Th and Tb.Sp values of NSPDr2 are higher than those of NSPDr and NSPDr1. For porosity of 25 to 65%, the mean values of Tb.Sp and Tb.Th NSP scaffolds were produced in the range of 0.15–0.74 mm and 0.21–0.73 mm. The Tb.Th and Tb.Sp values of the proposed NSP model design are the same in the natural cancellous bone range (Tb.Th = 0.081–1.89 mm and Tb.Sp = 0.148–5.085 mm), similar to the previous study [19]. The correlation between the mean of Tb.Th and Tb.Sp to tortuosity as shown in Figure 5(b). Figure 5(b) showed that increasing tortuosity, Tb.Sp decrease and for NSP model Tb.Th increase. The tortuosity of the NSP model is in the range of 1.41 – 2.75. These values are generally within the range of PDMS-based microchannel

with a tortuosity index of 1.57–2.30, giving the results of different migration velocities of the collective cells [20].

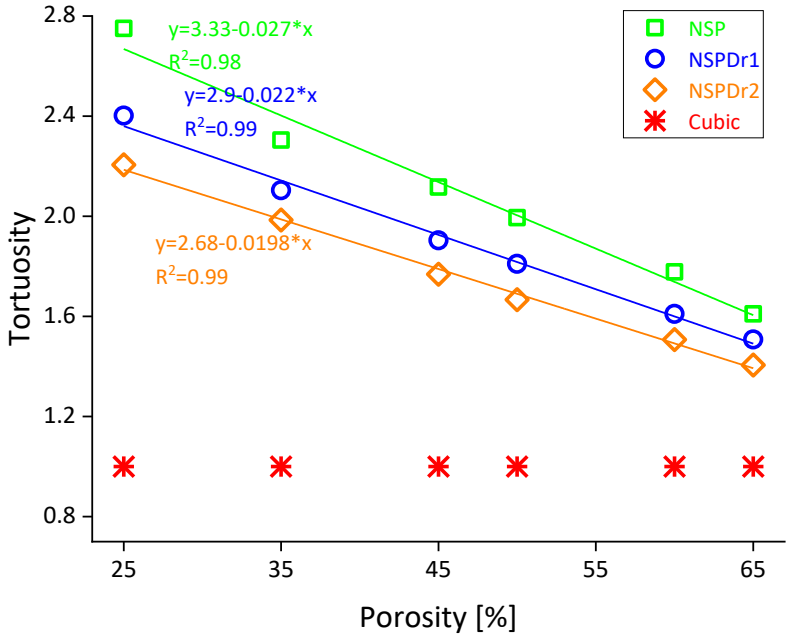

Fig. 4. Relation of porosity to tortuosity

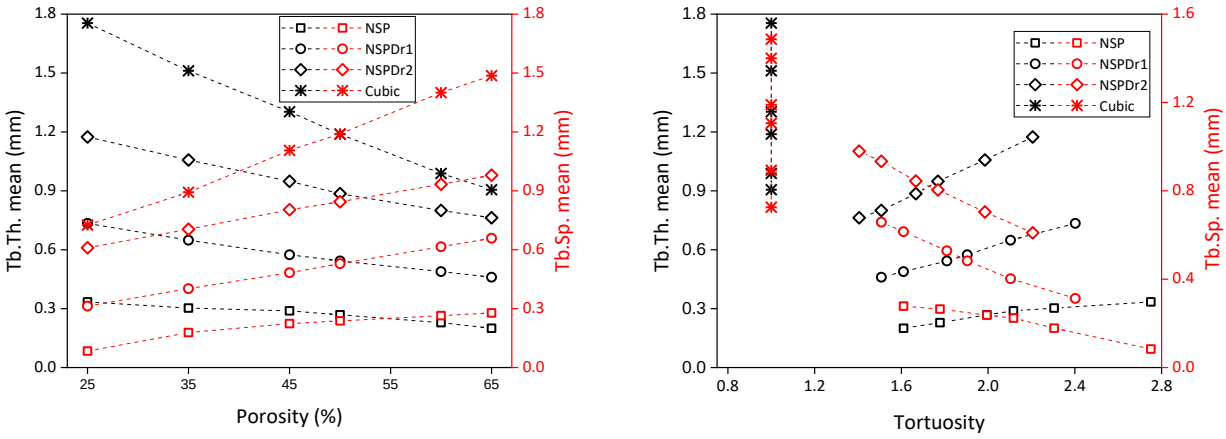

Fig. 5. (a) The relation of porosity to the trabecular thickness and trabecular separation; (b) The relation of porosity to the trabecular thickness and trabecular separation

Fig. **6**(a) shows the relationship of control parameters (porosity) to specific surface area; the prediction uses polynomial regression with R^2 = 99% of the overall NSP and NSPD models with different struth curvature. Based on Figure 7(a), the increasing porosity led to a phase where the specific surface area increases; in porosity. 25% to 45%, then drop at 50% to 75% porosity. In addition, rescaled NSP45 significantly increased the specific surface area (Fig. **6**(b)). The prediction of the relationship of tortuosity to the specific surface area with different NSP designs uses polynomial regression R^2 = 99% for each model. Based on Figure 7(b), the increases in tortuosity can potentially increase the specific surface area. Further, increasing the curvature parameter or the value of r in the design parameter decreases the specific surface area, tortuosity, and average values (Tb. Th); however, it increases the average value (Tb. Sp).

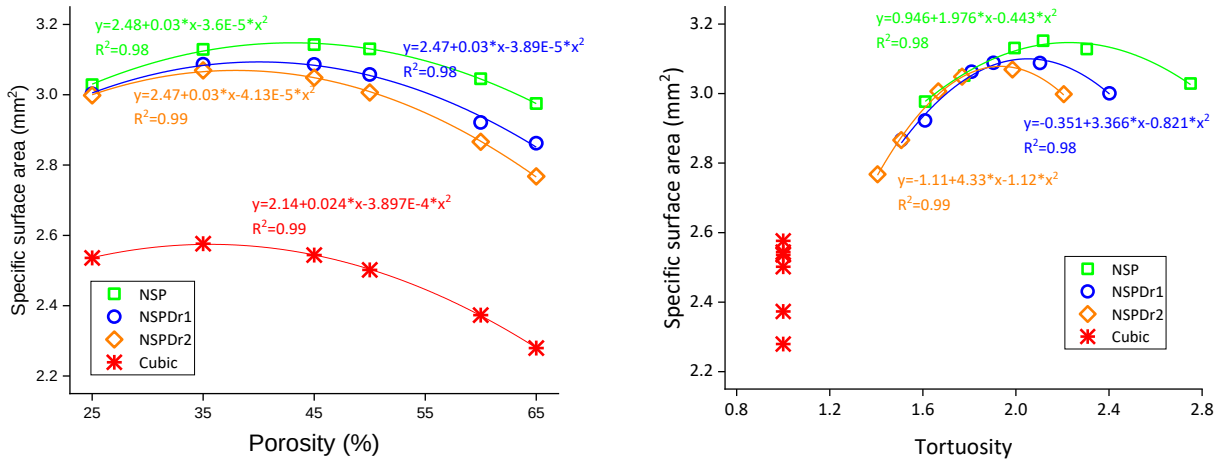

(a) (b)

Fig. 6. Relationship of specific surface areas to (a) Porosity; and (b) Tortuosity

3.3 CFD Results

Based on the simulation results in Figure 7(a), the porosity correlates with permeability; the prediction uses exponential regression with R^2 = 0.99 for each model. Figure 7(a) shows that increasing porosity gradually increases the permeability value. Whereas, for the cubic model at a porosity of 50%, the permeability is higher than the entire NSP model. In contrast to the relation of tortuosity to wall shear stress (Figure 7(b)), with increasing porosity, the wall shear stress decreases significantly.

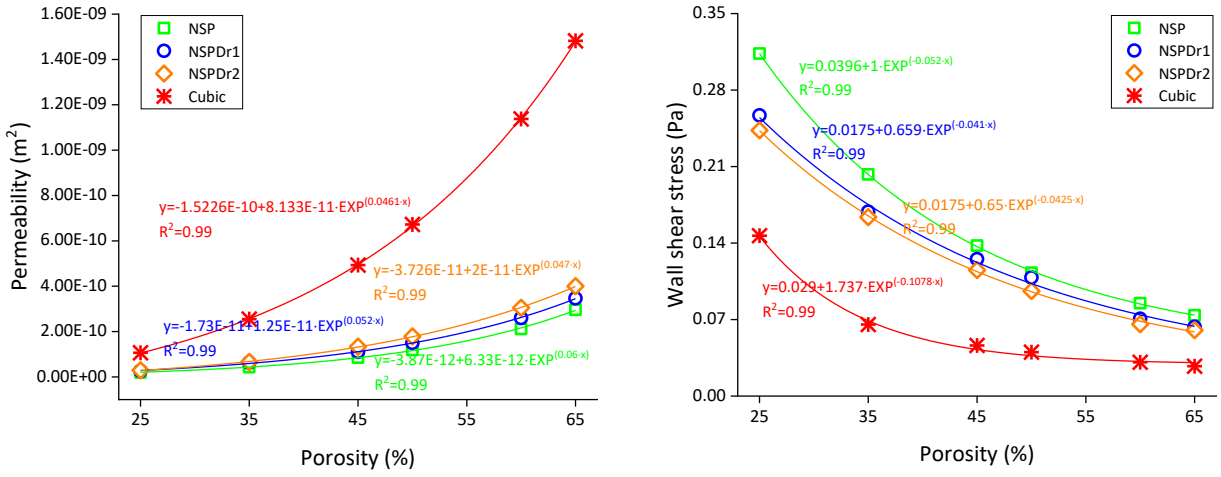

(a) (b)

Fig. 7. Relationship of porosity to (a) Permeability; (b) Wall shear stress

Fig. 8 shows the relationship of tortuosity to permeability and wall shear stress; the prediction uses exponential regression with R^2 = 0.99. Based on Figure 8(a), the tortuosity is allegedly a resistance for the fluid, shown in Figure 9. From Figure 8(a), increasing tortuosity decreases the permeability gradually. However, based on **Fig. 8**(b), it seems that tortuosity positively correlates with wall shear stress. From **Fig. 8**(b), increasing tortuosity significantly increases the wall shear stress. Manipulating the r value in the parametric design from 0.4 -0.49 mm can give different permeability and wall shear stress (although it is not very significant), even though they have the same porosity. The NSPDr2 model has a slightly higher permeability value than the overall porosity if compared to

the NSP and NSPDr1 models (**Fig. 8**(a)). In contrast, the NSPDr2 and NSPDr1 models have the lowest wall shear stress than the NSP model (**Fig. 8**(b)).

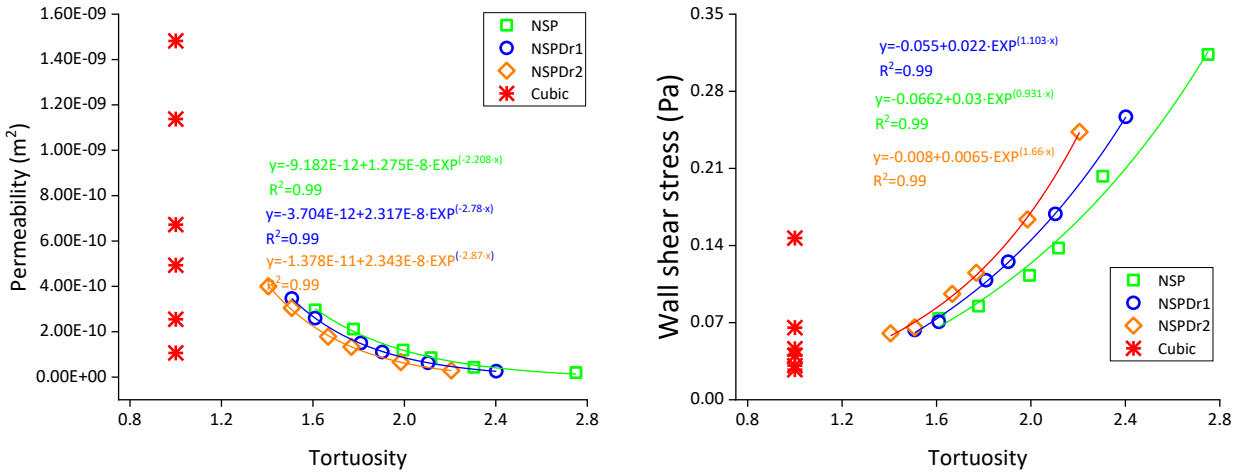

(a) (b)

Fig. 8. Relationship of tortuosity to (a) Permeability; (b) Wall shear stress

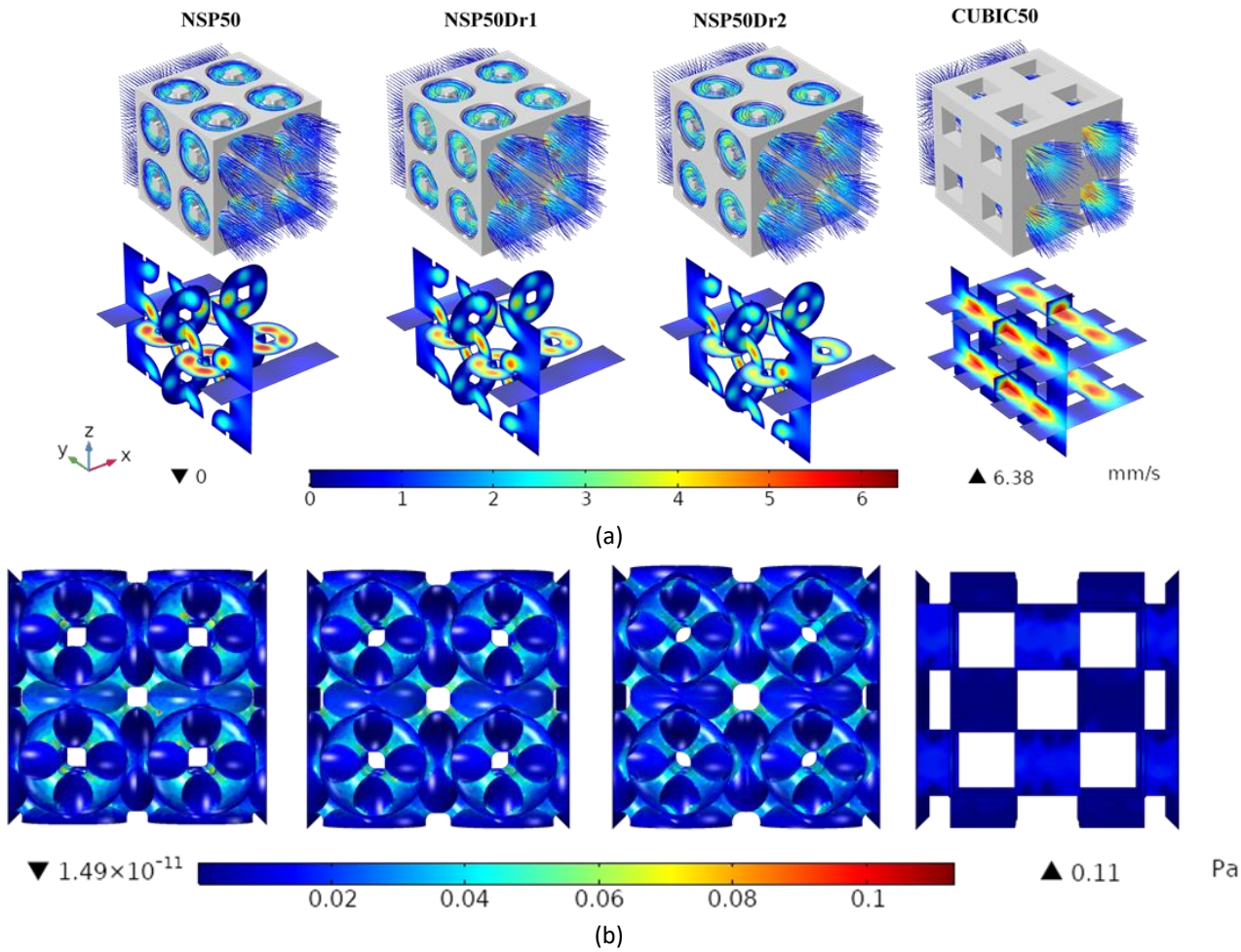

(a)

(b)

Fig. 9. (a) Velocity distribution; and (b) Fluid shear stress of porosity 50%

3.4 Discussion

The phenomenon of mass transport porous scaffolds study has been carried out with experimental and computational approaches to visualize fluid flow through bone scaffolds [21–25]; this is important since oxygen and nutrients have a significant role in cell survival and reproduction. Based on the previous study [26], the formation of mineralized tissue in the channel was driven by curvature significantly, where this hypothesis is similar to the results of this study. Based on morphology results, the radius of curvature affects the morphology of trabecular thickness, trabecular separation surface area, and tortuosity. The morphology significantly affects the mechanical behavior of bone [27–34]. The tortuosity has a good impact based on the results because it increases the specific surface area to the optimum phase and increases the fluid wall shear stress on the scaffold. From the overall structure of the NSP scaffold, the architecture of cancellous bone (Table 2) is contributed by nutrient transport. Increasing the porosity gives higher permeability but lowers the fluid wall shear stress. The controlling porosity and pore size that is too high may not positively impact the early stages of regeneration [7]. Then, the pore size must be in the range of 100 µm to 300 µm; if not, the cells will tend to congregate, thereby blocking oxygen and nutrients from getting to the center of the scaffold. Hence, too large a porosity will risk lowering the surface area.

Table 2
The comparison of the permeability of porous scaffolds and trabecular bones

No.	Model	Orientation	Permeability ($m^{2)}$
1	NSP25		$2.00\text{-}2.86 \times 10^{-11}$
2	NSP35		$4.68\text{-}6.84 \times 10^{-11}$
3	NSP45		$8.98 \times 10^{-11}\text{-}1.31 \times 10^{-10}$
4	NSP50		$1.207\text{-}1.786 \times 10^{-10}$
5	NSP60		$2.104\text{-}3046 \times 10^{-10}$
6	NSP65		$2.739\text{-}3.971 \times 10^{-10}$
7	CUBIC50		5.700×10^{-10}
8	bovine, distal femur(avg.) syahrom *et al.,* [23].	medial-lateral	0.03×10^{-10}
9	bovine, greater trochanter (avg.)	Align the axis of the femur	0.09×10^{-10}
10	bovine, neck of femur (avg.)	parallel along the axis	0.10×10^{-10}
11	Human vertebral body Nauman *et al.,* [35].	Longitudinal	8.50×10^{-10}
12	Human vertebral body	Transverse	3.59×10^{-10}
13	Human proximal femur	Longitudinal	2.76×10^{-10}
14	Human proximal femur	Transverse	1.20×10^{-10}
15	Human calcaneus	Medial–lateral	3.54×10^{-10}

The relationship between porosity and specific surface area is nonlinear, similar to the natural cancellous bone phenomenon [36]. The design to obtain the optimum specific value of the surface area facilitates the attachment of cells since seeding efficiency is highly dependent on the number of locations where cells attach to the scaffold matrix and the time available for cells to attach on the surface of the scaffold [37]. Hence, one possible solution is to include a winding path in the design of a scaffold with high porosity because, compared to a model with a straight path, a winding path may have a more positive impact. Since the model with a winding path will take longer or have a lower velocity to fall to the lowest point than the straight path.

Like the cubic model, designing a winding path will provide a longer path and a longer time for cells to interact with the scaffold matrix because tortuosity could increase the surface area and fluid

wall shear stress. The increased surface area of porous media affects increased cell adsorption (capillarity forces) for cells to penetrate micropores. Moreover, obtaining a more effective seeding efficiency is possible, allowing more cells throughout the proliferating scaffold to regenerate [38]. However, increasing the porosity will decrease the tortuosity. Hence, the NSP scaffold design that is proposed provides a suitable solution because the curvature can be controlled in such a way without affecting the porosity value. Table 2 compares the permeability of porous scaffolds and trabecular bones.

4. Conclusions

From the results, the design and biomaterial of the PLA scaffold proposed have fulfilled several aspects as an implant candidate. The permeability of the scaffold NSP model is similar in porosity. Then, the difference in curvature or tortuosity significantly increases the specific surface area and permeability. Providing a larger surface is more profitable because the cell seeding efficiency depends on the surface's availability to facilitate attachment. Further studies about fatigue are needed to predict the time of biomaterial damage and the wall shear stress studies on curvature variations to provide a bone scaffold design that can support the regeneration process. Then, the challenge for future research is to take advantage of the design potential by developing a scaffold with large porosity and curvature so that the tortuosity is large too.

Acknowledgement
The research/publication of this article was funded by DIPA of Public Service of Universitas Sriwijaya 2020. SP DIPA-023.17.2.677515/2022, revision 01, on March 16, 2020. In accordance with the Rector's Decree Number: 0685/UN9/SB.BUK.KP/2020, on July 15, 2020.

References
[1] Marinozzi, Franco, Fabiano Bini, and Andrea Marinozzi. "Evidence of entropic elasticity of human bone trabeculae at low strains." *Journal of biomechanics* 44, no. 5 (2011): 988-991. https://doi.org/10.1016/j.jbiomech.2010.11.030
[2] Marinozzi, Franco, Fabiano Bini, and Andrea Marinozzi. "Water uptake and swelling in single trabeculæ from human femur head." *Biomatter* 4, no. 1 (2014): e28237. https://doi.org/10.4161/biom.28237
[3] Gudekote, Manjunatha, and Rajashekhar Choudhari. "Slip effects on peristaltic transport of Casson fluid in an inclined elastic tube with porous walls." *Journal of Advanced Research in Fluid Mechanics and Thermal Sciences* 43, no. 1 (2018): 67-80.
[4] Marinozzi, Franco, Fabiano Bini, Annalisa De Paolis, Francesca Zuppante, Rossella Bedini, and Andrea Marinozzi. "A finite element analysis of altered load distribution within femoral head in osteoarthritis." *Computer Methods in Biomechanics and Biomedical Engineering: Imaging & Visualization* 3, no. 2 (2015): 84-90. https://doi.org/10.1080/21681163.2013.869185
[5] Marinozzi, Franco, Fabiano Bini, Annalisa De Paolis, Ramona De Luca, and Andrea Marinozzi. "Effects of hip osteoarthritis on mechanical stimulation of trabecular bone: a finite element study." *Journal of Medical and Biological Engineering* 35 (2015): 535-544. https://doi.org/10.1007/s40846-015-0061-4
[6] Roque, Waldir L., and Fabiano G. Wolf. "Computing the tortuosity of cancellous bone cavity network through fluid velocity field." In *XXIV Brazilian Congress on Biomedical Engineering-CBEB*, vol. 2014. 2014.
[7] Bobbert, F. S. L., and A. A. Zadpoor. "Effects of bone substitute architecture and surface properties on cell response, angiogenesis, and structure of new bone." *Journal of Materials Chemistry B* 5, no. 31 (2017): 6175-6192. https://doi.org/10.1039/C7TB00741H
[8] Karageorgiou, Vassilis, and David Kaplan. "Porosity of 3D biomaterial scaffolds and osteogenesis." *Biomaterials* 26, no. 27 (2005): 5474-5491. https://doi.org/10.1016/j.biomaterials.2005.02.002
[9] David, Bertrand, Dominique Bonnefont-Rousselot, Karim Oudina, Marie-Christelle Degat, Mickael Deschepper, Véronique Viateau, Morad Bensidhoum, Christian Oddou, and Hervé Petite. "A perfusion bioreactor for engineering bone constructs: an in vitro and in vivo study." *Tissue Engineering Part C: Methods* 17, no. 5 (2011): 505-516. https://doi.org/10.1089/ten.tec.2010.0468

[10] Ahsan, Tabassum, and Robert M. Nerem. "Fluid shear stress promotes an endothelial-like phenotype during the early differentiation of embryonic stem cells." *Tissue Engineering Part A* 16, no. 11 (2010): 3547-3553. https://doi.org/10.1089/ten.tea.2010.0014
[11] Sargent, Carolyn Y., Geoffrey Y. Berguig, Melissa A. Kinney, Luke A. Hiatt, Richard L. Carpenedo, R. Eric Berson, and Todd C. McDevitt. "Hydrodynamic modulation of embryonic stem cell differentiation by rotary orbital suspension culture." *Biotechnology and bioengineering* 105, no. 3 (2010): 611-626. https://doi.org/10.1002/bit.22578
[12] Adamo, Luigi, Olaia Naveiras, Pamela L. Wenzel, Shannon McKinney-Freeman, Peter J. Mack, Jorge Gracia-Sancho, Astrid Suchy-Dicey *et al.,* "Biomechanical forces promote embryonic haematopoiesis." *Nature* 459, no. 7250 (2009): 1131-1135. https://doi.org/10.1038/nature08073
[13] Delaine-Smith, Robin M., and Gwendolen C. Reilly. "Mesenchymal stem cell responses to mechanical stimuli." *Muscles, ligaments and tendons journal* 2, no. 3 (2012): 169.
[14] Jamali, Muhammad Sabaruddin Ahmad, Zuhaila Ismail, and Norsarahaida Saidina Amin. "Effect of Different Types of Stenosis on Generalized Power Law Model of Blood Flow in a Bifurcated Artery." *Journal of Advanced Research in Fluid Mechanics and Thermal Sciences* 87, no. 3 (2021): 172-183. https://doi.org/10.37934/arfmts.87.3.172183
[15] Chen, Ying, Shaoxiang Zhang, Jianan Li, Yang Song, Changli Zhao, and Xiaonong Zhang. "Dynamic degradation behavior of MgZn alloy in circulating m-SBF." *Materials Letters* 64, no. 18 (2010): 1996-1999. https://doi.org/10.1016/j.matlet.2010.06.011
[16] Voronov, Roman, Samuel VanGordon, Vassilios I. Sikavitsas, and Dimitrios V. Papavassiliou. "Computational modeling of flow-induced shear stresses within 3D salt-leached porous scaffolds imaged via micro-CT." *Journal of biomechanics* 43, no. 7 (2010): 1279-1286. https://doi.org/10.1016/j.jbiomech.2010.01.007
[17] Markhoff, Jana, Jan Wieding, Volker Weissmann, Juliane Pasold, Anika Jonitz-Heincke, and Rainer Bader. "Influence of different three-dimensional open porous titanium scaffold designs on human osteoblasts behavior in static and dynamic cell investigations." *Materials* 8, no. 8 (2015): 5490-5507. https://doi.org/10.3390/ma8085259
[18] Adanta, Dendy, Mochammad Malik Ibrahim, Dewi Puspita Sari, Imam Syofii, and Muhammad Amsal Ade Saputra. "Application of the Grid Convergency Index Method and Courant Number Analysis for Propeller Turbine Simulation." *Journal of Advanced Research in Fluid Mechanics and Thermal Sciences* 96, no. 2 (2022): 33-41. https://doi.org/10.37934/arfmts.96.2.3341
[19] Castro, A. P. G., R. B. Ruben, S. B. Gonçalves, J. Pinheiro, J. M. Guedes, and P. R. Fernandes. "Numerical and experimental evaluation of TPMS Gyroid scaffolds for bone tissue engineering." *Computer methods in biomechanics and biomedical engineering* 22, no. 6 (2019): 567-573. https://doi.org/10.1080/10255842.2019.1569638
[20] Mazalan, Mazlee Bin, Mohamad Anis Bin Ramlan, Jennifer Hyunjong Shin, and Toshiro Ohashi. "Effect of geometric curvature on collective cell migration in tortuous microchannel devices." *Micromachines* 11, no. 7 (2020): 659. https://doi.org/10.3390/mi11070659
[21] Bobbert, F. S. L., K. Lietaert, Ali Akbar Eftekhari, Behdad Pouran, S. M. Ahmadi, Harrie Weinans, and A. A. Zadpoor. "Additively manufactured metallic porous biomaterials based on minimal surfaces: A unique combination of topological, mechanical, and mass transport properties." *Acta biomaterialia* 53 (2017): 572-584. https://doi.org/10.1016/j.actbio.2017.02.024
[22] Kadir, Mohammed Rafiq Abdul, Ardiyansyah Syahrom, and Andreas Öchsner. "Finite element analysis of idealised unit cell cancellous structure based on morphological indices of cancellous bone." *Medical & biological engineering & computing* 48 (2010): 497-505. https://doi.org/10.1007/s11517-010-0593-2
[23] Syahrom, Ardiyansyah, Mohammed Rafiq Abdul Kadir, Muhamad Nor Harun, and Andreas Öchsner. "Permeability study of cancellous bone and its idealised structures." *Medical engineering & physics* 37, no. 1 (2015): 77-86. https://doi.org/10.1016/j.medengphy.2014.11.001
[24] Soufivand, Anahita Ahmadi, Nabiollah Abolfathi, Seyyed Ataollah Hashemi, and Sang Jin Lee. "Prediction of mechanical behavior of 3D bioprinted tissue-engineered scaffolds using finite element method (FEM) analysis." *Additive Manufacturing* 33 (2020): 101181. https://doi.org/10.1016/j.addma.2020.101181
[25] Truscello, Silvia, Greet Kerckhofs, Simon Van Bael, Grzegorz Pyka, Jan Schrooten, and Hans Van Oosterwyck. "Prediction of permeability of regular scaffolds for skeletal tissue engineering: a combined computational and experimental study." *Acta biomaterialia* 8, no. 4 (2012): 1648-1658. https://doi.org/10.1016/j.actbio.2011.12.021
[26] Vetsch, Jolanda R., Ralph Müller, and Sandra Hofmann. "The influence of curvature on three-dimensional mineralized matrix formation under static and perfused conditions: an in vitro bioreactor model." *Journal of The Royal Society Interface* 13, no. 123 (2016): 20160425. https://doi.org/10.1098/rsif.2016.0425
[27] Rincón-Kohli, Liliana, and Philippe K. Zysset. "Multi-axial mechanical properties of human trabecular bone." *Biomechanics and modeling in mechanobiology* 8 (2009): 195-208. https://doi.org/10.1007/s10237-008-0128-z

[28] Kaneko, Tadashi S., Jason S. Bell, Marina R. Pejcic, Jamshid Tehranzadeh, and Joyce H. Keyak. "Mechanical properties, density and quantitative CT scan data of trabecular bone with and without metastases." *Journal of biomechanics* 37, no. 4 (2004): 523-530. https://doi.org/10.1016/j.jbiomech.2003.08.010

[29] Majumdar, S., M. Kothari, P. Augat, D. C. Newitt, T. M. Link, J. C. Lin, T. Lang, Y. Lu, and H. K. Genant. "High-resolution magnetic resonance imaging: three-dimensional trabecular bone architecture and biomechanical properties." *Bone* 22, no. 5 (1998): 445-454. https://doi.org/10.1016/S8756-3282(98)00030-1

[30] Shim, V. P. W., L. M. Yang, J. F. Liu, and V. S. Lee. "Characterisation of the dynamic compressive mechanical properties of cancellous bone from the human cervical spine." *International Journal of Impact Engineering* 32, no. 1-4 (2005): 525-540. https://doi.org/10.1016/j.ijimpeng.2005.03.006

[31] Perilli, Egon, Massimiliano Baleani, C. Öhman, Roberta Fognani, Fabio Baruffaldi, and Marco Viceconti. "Dependence of mechanical compressive strength on local variations in microarchitecture in cancellous bone of proximal human femur." *Journal of biomechanics* 41, no. 2 (2008): 438-446. https://doi.org/10.1016/j.jbiomech.2007.08.003

[32] Teo, J. C. M., K. M. Si-Hoe, J. E. L. Keh, and S. H. Teoh. "Correlation of cancellous bone microarchitectural parameters from microCT to CT number and bone mechanical properties." *Materials Science and Engineering: C* 27, no. 2 (2007): 333-339. https://doi.org/10.1016/j.msec.2006.05.003

[33] Ford, Catherine M., and Tony M. Keaveny. "The dependence of shear failure properties of trabecular bone on apparent density and trabecular orientation." *Journal of biomechanics* 29, no. 10 (1996): 1309-1317. https://doi.org/10.1016/0021-9290(96)00062-0

[34] Schoenfeld, C. M., E. P. Lautenschlager, and P. R. Meyer. "Mechanical properties of human cancellous bone in the femoral head." *Medical and biological engineering* 12 (1974): 313-317. https://doi.org/10.1007/BF02477797

[35] Nauman, Eric A., K. E. Fong, and T. M. Keaveny. "Dependence of intertrabecular permeability on flow direction and anatomic site." *Annals of biomedical engineering* 27 (1999): 517-524. https://doi.org/10.1114/1.195

[36] Lerebours, Chloe, C. D. L. Thomas, J. G. Clement, P. R. Buenzli, and Peter Pivonka. "The relationship between porosity and specific surface in human cortical bone is subject specific." *Bone* 72 (2015): 109-117. https://doi.org/10.1016/j.bone.2014.11.016

[37] Van Bael, Simon, Yoke Chin Chai, Silvia Truscello, Maarten Moesen, Greet Kerckhofs, Hans Van Oosterwyck, J-P. Kruth, and J. J. A. B. Schrooten. "The effect of pore geometry on the in vitro biological behavior of human periosteum-derived cells seeded on selective laser-melted Ti6Al4V bone scaffolds." *Acta biomaterialia* 8, no. 7 (2012): 2824-2834. https://doi.org/10.1016/j.actbio.2012.04.001

[38] Yilgor, Pinar, Rui A. Sousa, Rui L. Reis, Nesrin Hasirci, and Vasif Hasirci. "Effect of scaffold architecture and BMP-2/BMP-7 delivery on in vitro bone regeneration." *Journal of Materials Science: Materials in Medicine* 21 (2010): 2999-3008. https://doi.org/10.1007/s10856-010-4150-1